Multispectral image fusion method based on intensity-hue-saturation and nonsubsampled three-channels non-separable wavelets

Bin Liu (刘 斌)[1*], Weijie Liu (刘维杰)[2], and Jiaxiong Peng (彭嘉雄)[3]

[1]*School of Mathematics and Computer Science, Hubei University, Wuhan 430062, China*

[2]*Computer School, Wuhan University, Wuhan 430079, China*

[3]*Institute of Image Recognition and Artificial Intelligence, Huazhong University of Science and Technology, Wuhan 430074, China*

[*]*E-mail: liubin3318@163.com*

Received July 22, 2009

A new multispectral image fusion method based on intensity-hue-saturation (IHS) transform and three-channel non-separable wavelets whose dilation matrix is [2,1;–1,1] is proposed. The multi-resolution decompositions of the intensity of multispectral image and panchromatic image are performed in nonsubsampled mode using the three-channel non-separable wavelet filter bank. The approximation images and the detail images of the multi-resolution pyramids are fused. The experimental results show that this method has good visual effect. The performance outperforms the IHS fusion method, the discrete wavelet transform (DWT) fusion method, and the IHS-DWT fusion method in preserving spectral quality and high spatial resolution information.

OCIS codes: 100.2000, 100.7410, 110.3000, 110.4234.

doi: 10.3788/COL20100804.0384.

The fusion of multispectral (MS) image integrates the images which have higher spectral quality but lower spatial resolution and the panchromatic images with higher spatial resolution. It creates a new image which has better spectral information and higher spatial resolution. It is a hot technology of remote sensing image fusion, and has been widely used[1,2].

A number of approaches to pixel-level fusion have been proposed for merging MS image and panchromatic image. The common procedures are intensity-hue-saturation (IHS) mergers[3], principal component analysis (PCA) mergers[4,5], Brovey transform mergers[6], separable discrete wavelet transform (DWT) mergers based on Mallat algorithm[7], and the Amélioration de la Résolution Spatiale par Injection de Structures (ARSIS) concept[8]. The fusion methods which are adopted most widely in MS image fusion are the IHS transform method and the DWT fusion method. But the two methods have their insufficiencies. The method of IHS transform can get high spatial resolution image, but the fused image may seriously lose the spectral information of the original MS image. A fused image with good spectral information can be created by the separable wavelet based on Mallat algorithm, but it is low in spatial resolution and there is block effect in the fused image because the subsampling is done when images are decomposed and reconstructed. To solve the problem, Zhang *et al*. proposed a fusion method combining IHS transform and DWT[9], and the fused image had good spectral quality and higher spatial resolution. But the mode of sub sampling by two is used in wavelet multi-resolution analysis, and the wavelet transform is not translation invariant. The block effect still exists in the fused image. Non-separable wavelet is a new kind of wavelet developed in recent years. Compared with the separable wavelet, it has many good characteristics and can get higher spatial resolution fusion result image. We have previously studied the multispectral image fusion methods based on four-channel and two-channel non-separable wavelets[10−12]. These methods have good fusion effect. However, compared with the fusion method based on four-channel non-separable wavelets, the fusion method based on three-channel non-separable wavelets has less computation amount while images are decomposed and reconstructed. Although the less computation amount is spent when the two-channel non-separable wavelets are applied to decompose and reconstruct images, less information is obtained because only the diagonal line elements of the two channel filters are non-zero[11,12]. In addition, the nonsubsampled non-separable wavelet transform is translation invariant, the fused images have good spectral quality and texture information without the block effect. Thus, to preserve good spectral information, higher spatial resolution, and reduce the computation amount of fusion process, a new fusion method based on three-channel non-separable wavelets is presented in this letter.

Let matrix M represent the sampling matrix. When M is equal to [2,1;–1,1], its determinant has an absolute value of three. According to the theory of general two-dimensional (2D) wavelet transform, there are three filters, i.e., a low-pass filter and two high-pass filters. Accordingly, there are one scale function and two wavelet functions. In this case, the (2D) scale function cannot be decomposed into the tensor product of two one-dimensional (1D) scale functions, and the wavelet functions cannot be decomposed into tensor product of two 1D wavelet functions or a scale function as well as a wavelet function.

Denote the low-pass filter as $H_0 = \{h_0(k)\}_{k\in Z^2}$ and the high-pass filters as $H_i = \{h_i(k)\}_{k\in Z^2} (i = 1, 2)$. The

decomposition process and the reconstruction process of three-channel non-separable wavelets are illustrated in Figs. 1 and 2, respectively, where A_{j+1}, A_j, and A_{j-1} are the approximation images of multi-scale decomposition corresponding to the scale indices $j+1$, j, and $j-1$; $D_j^{(1)}$, $D_j^{(2)}$ and $D_{j-1}^{(1)}$, $D_{j-1}^{(2)}$ are the detail images of the wavelet decomposition corresponding to the scale indices j and $j-1$; M is the sampling matrix; H_0, H_1, and H_2 are the low-pass filter (H_0) and the high-pass filters (H_1, H_2) of decomposition, respectively; H_0^*, H_1^*, and H_2^* are the low-pass filter and the high-pass filters of reconstruction corresponding to H_0, H_1, and H_2. Only two steps are given in the figures, and more steps can be given like this.

The downsampling process and the upsampling process are included in above flow charts. The non-separable wavelet transform in this case is not translation invariant. The texture information and spectral information cannot be preserved well. So the two processes are omitted in this research. The above process of decomposition and reconstruction also shows that the key problem of constructing non-separable wavelets is to construct the non-separable wavelet low-pass filter and high-pass filters. In the applications such as image fusion, when Mallat algorithm is used to decompose and reconstruct images, the concrete form of the scale function and the wavelet function are not involved in the decomposition and reconstruction of images. Hence, it is unnecessary to construct scale function and wavelet function. The main task is to construct the low-pass and high-pass filters of wavelet.

Nowadays, the design methods of 2D non-separable wavelets filter banks are focused on the wavelets of four channels and two channels. To our knowledge, the construction method of the 2D three-channel non-separable wavelet filter banks is not seen. According to the genaral constructing method of high dimensional wavelets with compact support and orthogonality[13], the construction of 2D three-channel non-separable wavelet filter banks is proposed as follows.

Constructing $X(x,y) = (1,x,y)$, $\mathrm{DG}(x,y) = \mathrm{Diag}(1, x^2/y, xy)$. For the sampling matrix $M = \begin{pmatrix} 2 & 1 \\ -1 & 1 \end{pmatrix}$, the form of the 2D three-channel non-separable wavelet filter banks with compact support and orthogonality is

$$\begin{aligned}&[m_0(x,y), m_1(x,y), m_2(x,y)]\\ =&\frac{1}{3}X(x,y)\prod_{j=1}^{K}[U_j\mathrm{DG}(x,y)U_j^{\mathrm{T}}]V,\end{aligned} \tag{1}$$

where $x = \mathrm{e}^{-\mathrm{i}\omega_1}$, $y = \mathrm{e}^{-\mathrm{i}\omega_2}$, $U_j (j = 1,2,\cdots,K)$ and $V/\sqrt{3} = (V_0, V_1, V_2)/\sqrt{3}$ are orthogonal matrices, V_1 and V_2 are 3×1 matrices, $V_0 = (1,1,1)^{\mathrm{T}}$.

To seek 4×4 filter banks, letting K=1, We can construct

$$C_1 = \begin{pmatrix} \cos(\alpha_1) & -\sin(\alpha_1) & 0 \\ \sin(\alpha_1) & \cos(\alpha_1) & 0 \\ 0 & 0 & 1 \end{pmatrix},$$

$$C_2 = \begin{pmatrix} 1 & 0 & 0 \\ 0 & \cos(\alpha_2) & -\sin(\alpha_2) \\ 0 & \sin(\alpha_2) & \cos(\alpha_2) \end{pmatrix},$$

$$C_3 = \begin{pmatrix} 0 & 0 & 1 \\ \cos(\alpha_3) & -\sin(\alpha_3) & 0 \\ \sin(\alpha_3) & \cos(\alpha_3) & 0 \end{pmatrix},$$

$$C_4 = \begin{pmatrix} 0 & \cos(\alpha_4) & -\sin(\alpha_4) \\ 0 & \sin(\alpha_4) & \cos(\alpha_4) \\ 1 & 0 & 0 \end{pmatrix},$$

$$C_5 = \begin{pmatrix} \cos(\alpha_5) & 0 & -\sin(\alpha_5) \\ 0 & 1 & 0 \\ \sin(\alpha_5) & 0 & \cos(\alpha_5) \end{pmatrix},$$

$$V = \begin{pmatrix} 1 & -\sqrt{2}/2 & -\sqrt{6}/2 \\ 1 & \sqrt{2} & 0 \\ 1 & -\sqrt{2}/2 & \sqrt{6}/2 \end{pmatrix}.$$

Taking

$$U_1 = C_1C_2C_3C_4C_5, \tag{2}$$

it can be validated that $U_1\,(\alpha_j (j = 1,2,\cdots,5)$ are the parameters) and $V/\sqrt{3}$ are orthonormal matrices. The number of filter banks is infinite according to Eq. (2) with different values of α_j. We have designed many filter banks with compact support and orthonormality. We give an example here:

$$H_0 = \begin{pmatrix} 0 & 0 & 0.0392 & -0.0226 \\ 0.3763 & 0.1694 & 0.3434 & 0 \\ -0.0318 & -0.0821 & 0.1865 & 0 \\ 0 & 0.0216 & 0 & 0 \end{pmatrix},$$

$$H_1 = \begin{pmatrix} 0 & 0 & -0.0329 & 0.0190 \\ -0.0030 & -0.0013 & -0.2886 & 0 \\ 0.0003 & -0.1998 & 0.4538 & 0 \\ 0 & 0.0526 & 0 & 0 \end{pmatrix},$$

$$H_2 = \begin{pmatrix} 0 & 0 & -0.0405 & 0.0234 \\ 0.3659 & 0.1647 & -0.3555 & 0 \\ -0.0309 & 0.0828 & -0.1881 & 0 \\ 0 & -0.0218 & 0 & 0 \end{pmatrix}. \tag{3}$$

It can be validated that this is an orthonormal filter bank. H_0, H_1, and H_2 are all non-separable.

The fusion algorithm is given below.

Step 1: Registering the MS image and panchromatic image.

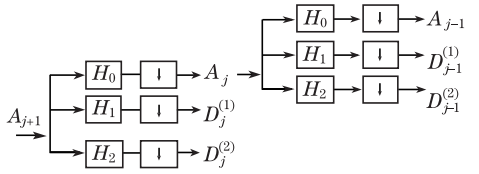

Fig. 1. Three-channel non-separable wavelet decomposition of image.

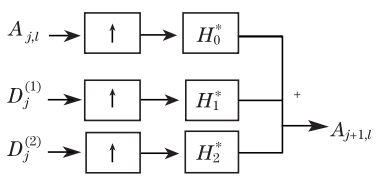

Fig. 2. Three-channel non-separable wavelet reconstruction of image.

Step 2: Performing IHS transform to the original MS image:

$$\begin{bmatrix} I \\ v_1 \\ v_2 \end{bmatrix} = \begin{bmatrix} 1/3 & 1/3 & 1/3 \\ -\sqrt{2}/6 & -\sqrt{2}/6 & 2\sqrt{2}/6 \\ 1/\sqrt{2} & -1/\sqrt{2} & 0 \end{bmatrix} \begin{bmatrix} R \\ G \\ B \end{bmatrix}, \quad (4)$$

$$H = \arctan \frac{v_2}{v_1}, \quad (5)$$

$$S = \sqrt{v_1^2 + v_2^2}, \quad (6)$$

where I denotes intensity, H denotes hue, and S denotes saturation.

Step 3: Performing histogram matching between the panchromatic image and the intensity component of the MS image. Let I be the intensity component of the original MS image, the average value of I is m_1, and its standard variance is σ_1. Let P be the panchromatic image, the average value of P is m_2, and its standard variance is σ_2. Then the macthing process can be described as

$$P' = \frac{\sigma_1}{\sigma_2} P + m_1 - \frac{\sigma_1}{\sigma_2} m_2. \quad (7)$$

Step 4: Fusing I and P' and generating the fused image I'. We perform multi-resolution non-separable wavelet decomposition to the images I and P' according to the process described in Fig. 1 using the filter bank (3). To avoid blocking artifacts in the fused image, we omit the downsampling process. The detail components of I are replaced by the corresponding level detail components of P'. The selective method of approximation components is essential for the fused image to get good spectral information and high spatial resolution. Denoting the approximation components of I and P' as IA and $P'A$, respectively, the linear representation of the approximation component of the fused image is

$$FA = t \times IA + (1 - t) \times P'A, \quad (8)$$

where $t\,(0 \le t \le 1)$ is the adjustive parameter. When t changes greater, the spectral information of the fused image changes better. Ohterwise, the spatial resolution changes higher. To get the fused image with good spectral resolution and high spatial resolution, we select $t = 1/2$, and the low-frequency image of the highest layer is the average of IA and $P'A$.

Then we perform the non-separable wavelet inverse transform and reconstruct the new intensity image F according to the nonsubsampled mode.

Step 5: Performing IHS inverse transform to F, H, S and generating the fused multispectral image.

We performed experiments for the fusion of LISS-3 images taken from IRS-P6 satellite. Figure 3(a) is the source LISS-3 panchromatic image whose spatial resolution is 5.8 m, and Fig. 3(b) is the source LISS-3 multi-band image whose spatial resolution is 23.5 m. The three bands are the B2 band (green), the B3 band (red), and the B4 band (near infrared). This is a fire scene. Flame is burning on the upper right corner and is extinguished on the lower-left corner of the scene. The traces of burning are left.

Figure 3(f) is the fused image of the proposed fusion method. In order to see the fusion effects clearly, we compare this method with the fusion methods based on IHS transform[3], DWT[7] and IHS-DWT[9]. Figures 3(c), (d), and (e) are the fused images of the three fusion methods, respectively. The wavelet function used in DWT is the tensor product of db2 which is the second wavelet of Daubechies series wavelets, and it has the same length as $H_i\,(i = 0, 1, 2)$. The numbers of decomposition layers of the methods based on DWT, IHS-DWT, and the proposed method are three, and the experiment is realized in the programming environment of MATLAB 7.5.

From the comparison of visual effect, it is found that the fused image of the proposed fusion method can preserve good spectral information and higher spatial resolution. The flame color and the traces of burning of the scene are unartificial. It has no blocking artifact in the fused image. The fused images based on IHS fusion method (Fig. 3(c)) has high spatial resolution, but the spectral information is distorted badly. The fused images based on DWT and IHS-DWT also have good spectral information, but there are marked block effects in the ridge and other places.

The bias index (BIAS), the standard deviation (SD), the correlation coefficients between the fused image and the source MS image (CC), the relative average spectral error (RASE), and the relative global dimensional synthesis error (ERGAS) are used to measure the spectral information contained in the fused images[14]. The smaller the values of BIAS, SD, RASE, and ERGAS are, the better the spectral information preservation is. The larger the value of CC, the better the spectral

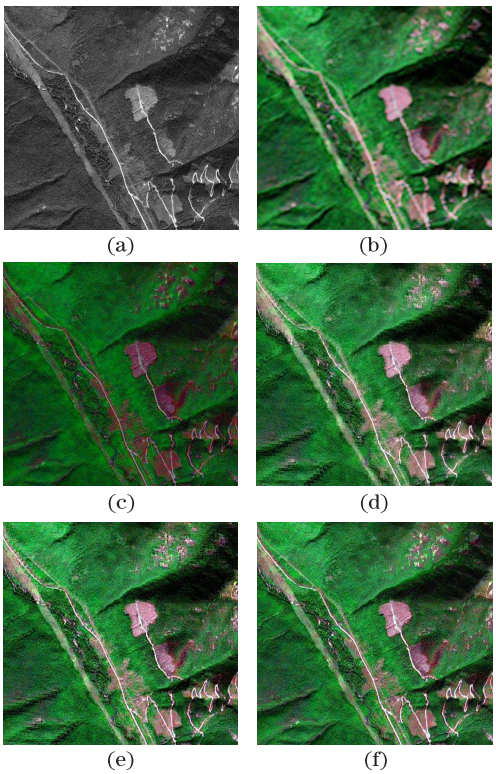

Fig. 3. Fusion of LISS-3 MS image and panchromatic image. (a) Original panchromatic image; (b) original MS image; (c) IHS fused image; (d) DWT fused image; (e) IHS-DWT fused image; (f) fused image of the proposed method

Table 1. Performance Indices of LISS-3 Fused Images

	IHS Method			DWT Method			IHS-DWT Method			Proposed Method		
	R	G	B	R	G	B	R	G	B	R	G	B
BIAS	28.12	33.36	32.66	17.93	17.24	15.88	16.60	18.12	17.45	15.09	16.19	15.78
SD	41.78	42.58	42.51	27.02	23.79	22.86	23.99	24.79	24.63	21.42	22.05	21.92
RASE		49.22			5.590			1.925			1.335	
ERGAS		154.29			11.80			3.872			3.095	
CC	0.860	0.709	0.718	0.870	0.864	0.853	0.888	0.836	0.820	0.910	0.866	0.854
Entropy	5.949	6.793	6.010	7.004	7.506	7.129	7.090	7.439	7.100	7.108	7.510	7.131
sCC	0.934	0.972	0.986	0.937	0.976	0.968	0.966	0.987	0.981	0.973	0.989	0.985

information preservation.

The entropy and a kind of correlation coefficients (sCC) are used to measure the high spatial information preserved in the fused images[14]. The high sCC between the fused image and the panchromatic image indicates that most of the spatial information of the panchromatic image has been incorporated during the fusion process.

Table 1 lists the objective performance indices of the fused images using IHS method, DWT method, IHS-DWT method, and the proposed method. The BIAS, SD, RASE, ERGAS values of the proposed method are smaller than those of the other three methods, while the CC, entropy, and sCC values are greater than those of the other three methods. It shows that the proposed fusion method outperforms the IHS fusion method, DWT fusion method, and IHS-DWT fusion method in preserving good spectral information and high spatial resolution.

In addition, the same conclusion is gotten when other non-separable wavelet filter banks are used to fuse LISS-3 MS image and panchromatic image.

In conclusion, a new image fusion method of MS image and panchromatic image based on three-channel non-separable wavelet whose dilation matrix is [2,1;–1,1] is presented. A construction method of filter bank about this kind of wavelet is presented. Non-separable low-pass and high-pass filters are constructed. The proposed method has good fusion vision effect. The fusion performance of the method proposed outperforms the fusion method based on IHS, DWT, and IHS-DWT in perserving good spectral information and high spatial resolution information.

When using the methods proposed in this letter to fuse the SPOT-XS image and the SPOT-PAN image, or the SPOT high spatial resolution image and TM MS image, the same conclusion can be obtained. The amount of computation is reduced to about three quarters of the fusion method based on four-channel non-separable wavelets.

This work was supported by the National Natural Science Foundation of China (No. 10477007) and the Key Project of the Natural Science Foundation of Hubei Province (No. 2009CDA133).

References

1. C. Thomas, T. Ranchin, L. Wald, and J. Chanussot, IEEE Trans. Geosci. Remote Sens. **46,** 1301 (2008).
2. Q. Zhang and B. Guo, Acta Opt. Sin. (in Chinese) **28,** 74 (2008).
3. P. S. Chavez, Jr., S. C. Sides, and J. A. Anderson, Photogramm. Eng. Remote Sens. **57,** 295 (1991).
4. V. K. Shettigara, Photogramm. Eng. Remote Sens. **58,** 561 (1992).
5. Q. Miao and B. Wang, Chin. Opt. Lett. **6,** 104 (2008).
6. T.-M. Tu, S.-C. Su, H.-C. Shyu, and P. S. Huang, Information Fusion **2,** 177 (2001).
7. D. A. Yocky, J. Opt. Soc. Am. A **12,** 1834 (1995).
8. T. Ranchin and L. Wald, Photogramm. Eng. Remote Sens. **66,** 49 (2000).
9. Y. Zhang and G. Hong, Information Fusion **6,** 225 (2005).
10. B. Liu and J. Peng, Chin. J. Computers (in Chinese) **32,** 350 (2009).
11. B. Liu and J. Peng, Science in China Series F: Information Sciences **51,** 2022 (2008).
12. B. Liu and J. Peng, Acta Opt. Sin. (in Chinese) **27,** 1419 (2007).
13. Q. Chen, C. A. Micchelli, S. Peng, and Y. Xu, SIAM J. Matrix Anal. Appl. **25,** 517 (2003).
14. M. Choi, R. Y. Kim, M.-R. Nam, and H. O. Kim, IEEE Geosci. Remote Sens. Lett. **2,** 136 (2005).